Biochimica et Biophysica Acta 1828 (2013) 732–742

Contents lists available at SciVerse ScienceDirect

Biochimica et Biophysica Acta

journal homepage: www.elsevier.com/locate/bbamem

Transmembrane pore formation by the carboxyl terminus of Bax protein

Pranav Garg [a,b], Kathleen N. Nemec [c], Annette R. Khaled [c], Suren A. Tatulian [a,*]

[a] Department of Physics, College of Sciences, University of Central Florida, Orlando, FL, USA
[b] Biotechnology Graduate Program, College of Medicine, University of Central Florida, Orlando, FL, USA
[c] Burnett School of Biomedical Sciences, College of Medicine, University of Central Florida, Orlando, FL, USA

ARTICLE INFO

Article history:
Received 28 February 2012
Received in revised form 29 July 2012
Accepted 7 August 2012
Available online 18 August 2012

Keywords:
Peptide
Membrane pore
Kinetics
Calcein release
Oligomeric state

ABSTRACT

Bax is a cytosolic protein that responds to various apoptotic signals by binding to the outer mitochondrial membrane, resulting in membrane permeabilization, release of cytochrome *c*, and caspase-mediated cell death. Currently discussed mechanisms of membrane perforation include formation of hetero-oligomeric complexes of Bax with other pro-apoptotic proteins such as Bak, or membrane insertion of multiple hydrophobic helices of Bax, or formation of lipidic pores physically aided by mitochondrial membrane-inserted proteins. There is compelling evidence provided by our and other groups indicating that the C-terminal "helix 9" of Bax mediates membrane binding and pore formation, yet the mechanism of pore forming capability of Bax C-terminus remains unclear. Here we show that a 20-amino acid peptide corresponding to Bax C-terminus (VTIFVAGVLTASLTIWKKMG) and two mutants where the two lysines are replaced with glutamate or leucine have potent membrane pore forming activities in zwitterionic and anionic phospholipid membranes. Analysis of the kinetics of calcein release from lipid vesicles allows determination of rate constants of pore formation, peptide–peptide affinities within the membrane, the oligomeric state of transmembrane pores, and the importance of the lysine residues. These data provide insight into the molecular details of membrane pore formation by a Bax-derived peptide and open new opportunities for design of peptide-based cytotoxic agents.

1. Introduction

Cellular homeostasis is regulated by cell renewal and apoptosis. Various apoptotic stimuli result in recruitment of B cell lymphoma 2 (BCL-2) family proteins to mitochondria, outer mitochondrial membrane permeabilization, release of cytochrome *c*, followed by caspase-mediated cell death [1–4]. Formation of mitochondrial membrane pores is a critical step, considered a point of no return in terms of cell life or death [2,3,5]. The existing evidence suggests that pro-apoptotic Bax, truncated Bid, and Bak proteins form hetero-oligomeric structures in mammalian cells upon activation that are directly involved in mitochondrial membrane permeabilization [6–12]. The process is mediated by Ca^{2+} ions and probably involves intermolecular disulfide bridging as Ca^{2+} and truncated Bid promoted Bax binding to isolated mitochondria, oligomerization, and cytochrome *c* release, while dithiothreitol inhibited the effect [13]. However, even in the absence of Ca^{2+} and truncated Bid, Bax was able to bind to mitochondria and form homo-oligomers with aggregation numbers of 2 to 5 and higher [13]. Consistent with this, recombinantly expressed and purified Bax was shown to form oligomeric structures in phospholipid membranes and cause leakage of 8-amino-naphthalene-1,3,6-trisulfonic acid ($M_r \approx 384$) from lipid vesicles in the absence of any accessory factors [14]. These data indicate that Bax indeed possesses an intrinsic propensity and capability of membrane pore formation.

Structural similarity between certain BCL-2 family proteins, including Bax, and bacterial toxins such as colicin and diphtheria toxin that form endosome membrane pores at acidic pH [1,15,16] has prompted studies on membrane pore formation by Bax and its pH dependence [17–21]. Functional studies involving point and deletion mutagenesis, as well as the NMR structure of Bax, suggested that the hydrophobic C-terminal α-helix 9 of Bax, and possibly helices 5 and 6, insert into the mitochondrial membrane upon apoptosis thus promoting pore formation [1,10,22–27]. Bax with deleted C-terminus ($Bax_{\Delta C}$) was incapable of mitochondrial membrane binding and permeabilization [22–24], yet this truncated version of Bax was used in many studies because the removal of the "hydrophobic tail" rendered the protein water soluble and eased its handling [17–21]. $Bax_{\Delta C19}$ (*i.e.* Bax lacking C-terminal 19 residues)

Abbreviations: BaxC-KK, C-terminal peptide of wild-type Bax protein: Ac-VTIFVAGVLTASLTIWKKMG-NH_2; BaxC-EE, C-terminal peptide of Bax protein with two lysines replaced by glutamates; BaxC-LL, C-terminal peptide of Bax protein with two lysines replaced by leucines; BCL-2, B cell lymphoma 2; DPC, dodecylphosphocholine; LUV, large unilamellar vesicle; POPC, 1-palmitoyl-2-oleoyl-*sn*-glycero-3-phosphocholine; POPG, 1-palmitoyl-2-oleoyl-*sn*-glycero-3-phosphoglycerol

* Corresponding author at: Department of Physics, Physical Sciences Room 456, University of Central Florida, 4000 Central Florida Boulevard, Orlando, FL 32816-2385, USA. Tel.: +1 407 823 6941; fax: +1 407 823 5112.
E-mail address: statulia@ucf.edu (S.A. Tatulian).

0005-2736/$ – see front matter © 2012 Elsevier B.V. All rights reserved.
http://dx.doi.org/10.1016/j.bbamem.2012.08.006

formed Cl^--selective pores in lipid membranes that reached maximum conductivity around pH 4.0 [18]. This echoes with results obtained on $Bax_{\Delta C20}$, which caused maximal release of carboxyfluorescein ($M_r \approx 326$) from phospholipid vesicles at acidic pH of ~4.0, but is in conflict with formation of cation-selective channels that were suppressed at acidic pH [17]. Strong potency of $Bax_{\Delta C19}$ to release carboxyfluorescein, cytochrome *c* ($M_r \approx 11{,}749$), and large dextran molecules ($M_r \geq 6000$) from lipid vesicles was demonstrated [20]. These latter data implied that $Bax_{\Delta C19}$ was able to form tetrameric pores in lipid membranes with a diameter of 22 Å to 30 Å [16,20]. Membrane pore formation by $Bax_{\Delta C}$ accords with its ability to release cytochrome *c* from isolated mitochondria [19], but is not consistent with data indicating inability of $Bax_{\Delta C}$ to localize to mitochondria and promote apoptosis [22–24] or to release carboxyfluorescein from lipid vesicles [21]; the latter studies indicated that the C-terminal stretch of Bax was necessary for its *in vivo* membrane permeabilization function. Yet another study demonstrated that $Bax_{\Delta C20}$ could form only small pores in lipid vesicles, and addition of truncated Bid resulted in release of fluorescein-conjugated dextrans of $M_r \sim 70{,}000$ [25]. Furthermore, oligomeric full-length Bax (*i.e.* Bax solubilized in octylglucoside) made pores in isolated mitochondrial membranes or in lipid vesicles that could transfer cytochrome *c* and dextran molecules as large as $M_r \sim 2 \times 10^6$ [7,26], but untreated (monomeric) Bax was unable to form pores large enough to transport cytochrome *c* even when aided by truncated Bid [21].

In full-length Bax, the C-terminal helix 9 is located in a hydrophobic groove [27]. This location is stabilized by H-bonding between Ser^{184} and Asp^{98} and disruption of this H-bonding is thought to allow disengagement of the C-terminus and insertion into the mitochondrial membrane during apoptosis [1,23]. Logically, the isolated C-terminal peptide would insert into lipid membranes and cause membrane leakage. A synthetic peptide corresponding to Bax C-terminal 21 residues was indeed shown to bind to phospholipid vesicles and release vesicle-entrapped carboxyfluorescein [28,29]. Moreover, our recent efforts to develop peptide-based cytotoxic agents identified that the C-terminal 20-residue peptide of Bax, when delivered *via* polymeric nanoparticles, is capable of efficiently killing breast and colon cancer cells, accompanied with mitochondrial membrane hyperpolarization and plasma membrane rupture [30]. Intratumoral or intravenous injections of the nanoparticle-encapsulated peptide resulted in significant tumor regression in mice within 4–9 days, and mutations of the two lysines to neutral or acidic residues strongly altered the cytotoxic properties of the peptide. Despite the evidence for the strong potency of Bax C-terminal peptide to kill cells through a mechanism involving perturbations of the mitochondrial membrane, the molecular details of membrane pore formation by the peptide, such as the kinetics of pore formation and the oligomeric state of the pore, remain unclear.

The aim of this study is to analyze the membrane pore formation mechanism by Bax C-terminal 20-residue peptide. The wild-type peptide, as well as two mutants where the two lysines are replaced either with glutamates (charge reversal) or leucines (charge neutralization), form relatively large pores in zwitterionic and anionic membranes. Consistent with the cytotoxic effect of the peptide on cancer cells (see above), the most efficient pores are formed by the wild-type peptide in anionic membranes. The kinetics of calcein ($M_r \approx 623$) release at various concentrations of the three peptides allowed identification of the second-order rate constants of pore formation within the membrane, the affinity constants of pore forming peptide units, and the oligomeric pore structure. Nucleation of the pore is shown to be relatively slow and involve 2–3 peptide molecules, followed by a faster process of assembly of the pore that includes up to eight peptide molecules. It is clearly realized that *in vitro* data on the behavior of the isolated peptide may not directly reflect the mechanism of the full length Bax protein. However, our efforts to analyze peptide-mediated cell death and the molecular basis of formation of large membrane pores may facilitate design of peptide-based cytolytic agents to eliminate detrimental cells such as bacteria, fungi, or cancer cells.

2. Materials and methods

2.1. Materials

The lipids, 1-palmitoyl-2-oleoyl-*sn*-glycero-3-phosphocholine (POPC), 1-palmitoyl-2-oleoyl-*sn*-glycero-3-phosphoglycerol (POPG), and dodecylphosphocholine (DPC) were purchased from Avanti Polar Lipids, Inc. (Alabaster, AL). Bax C-terminal peptide, named BaxC-KK (Ac-VTIFVAGVLTASLTIWKKMG-NH_2), and the two mutants where lysines at positions 17 and 18 were replaced with glutamic acid or leucine residues (BaxC-EE and BaxC-LL, respectively) were purchased from Biopeptide Co., Inc. (San Diego, CA) and were >98% pure as documented by HPLC and mass-spectrometry. The N- and C-termini of the peptides were acetylated and amidated, respectively, to eliminate the electrostatic effects of the terminal charges on the peptide behavior.

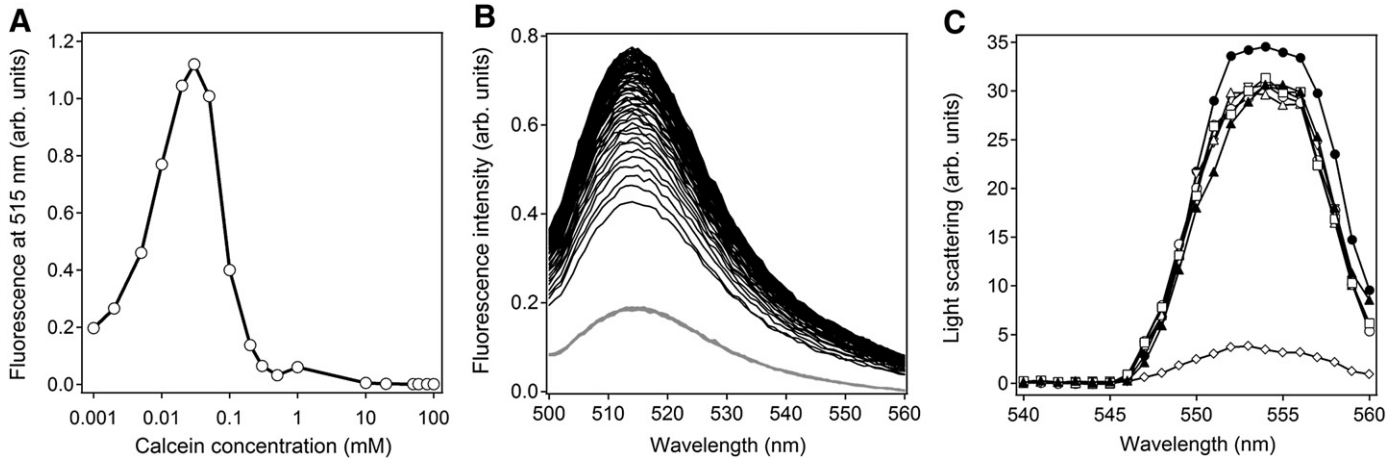

Fig. 1. Calcein is self-quenched at high concentrations, and peptides do not cause vesicle rupture. A: Concentration dependence of calcein fluorescence. Excitation wavelength and bandwidth were 490 nm and 2 nm, and emission wavelength and bandwidth were 515 nm and 10 nm, respectively. Average values and standard deviations of fluorescence intensities were generated by three independent experiments. B: Progression of calcein fluorescence spectra upon addition of 1.667 μM BaxC-KK peptide to POPC vesicles (at 0.5 mM total lipid concentration) loaded with 10 mM calcein. Gray lines at the lower part of the graph show the spectra before peptide addition, and the black lines correspond to spectra measured following peptide addition, with periodicity of 20 s per spectrum. C: Light scattering at right angle from 10 mM calcein-loaded POPC vesicles (closed circles), and following addition of 10% buffer (inverted triangles), 0.6 mM DPC (closed triangles), 1.667 μM (open triangles), 5.0 μM (squares), and 15.0 μM (open circles) of BaxC-KK peptide, or 0.05% Triton X-100 (rhombs). The peptide has been initially solubilized in 6.0 mM DPC at a 10-fold concentration so dilution into the vesicle suspension yielded the indicated concentrations. Temperature was 37 °C, and all samples were in 20 mM Na,K-phosphate, 150 mM NaCl, and 0.8 mM EGTA, pH 7.2.

Sephadex G-50 resin was from GE Healthcare Bio-Sciences Corp. (Piscataway, NJ) and SM-2 Bio-beads were from Bio-Rad Laboratories (Hercules, CA). Calcein disodium salt and other chemicals were of analytical grade and of the highest purity and were purchased from Sigma-Aldrich (St. Louis, MO). Polycarbonate filters for extruded lipid vesicle preparation were purchased from Avestin, Inc. (Ottawa, Ontario, Canada).

2.2. Calcein release assay

Large unilamellar vesicles (LUVs) were prepared by extrusion of the lipid suspension through 200 nm pore-size polycarbonate filters, as described [31], using 100% POPC or 70% POPC + 30% POPG, at a total lipid concentration of 10 mM in an aqueous buffer containing 20 mM Na,K-phosphate, 150 mM NaCl, 0.8 mM EGTA, pH 7.2, and 10 mM calcein disodium salt. Calcein at 10 mM has been shown to yield little fluorescence because of self-quenching [32]. Vesicles were separated from calcein in the external medium by passing the sample through a Sephadex G-50-packed desalting column (10 in. by 0.7 in.) equilibrated with the same buffer without calcein. The flow rate was set at 1.0 mL/min using a peristaltic pump and 0.15 mL calcein-loaded vesicle fractions were collected. The lipid concentration was evaluated by measuring the right angle static light scattering of the lipid vesicle suspension at 550 nm and comparing with a calibration curve. The final lipid concentration was adjusted to 0.5 mM by adding plane (calcein-free) buffer. The kinetics of calcein release from LUVs was studied by measuring consecutive fluorescence spectra between 500 and 560 nm with 20 s periodicity, at 37 °C, on a J-810 spectrofluoropolarimeter (Jasco, Inc., Tokyo, Japan) equipped with a PFD-425S Peltier temperature controller. The excitation was at 490 nm, and the excitation and emission bandwidths were 2 nm and 10 nm, respectively. Before addition of the peptide, little fluorescence was recorded because of self-quenching of calcein at 10 mM. At 5 min into the measurements, a 1/10th volume of the peptide solubilized in 6.0 mM DPC in a buffer of 20 mM Na,K-phosphate, 150 mM NaCl, 0.8 mM EGTA, pH 7.2, was added to calcein-loaded vesicles, followed by dispersion of DPC below its cmc (~1.5 mM), transfer of the peptide into the vesicle membranes, and calcein release, which was detected by measurements of consecutive fluorescence spectra for 25 more minutes. Membrane pore formation capabilities were studied for the three peptides, *i.e.*, the wild-type peptide BaxC-KK and the two mutant peptides BaxC-EE and BaxC-LL. Three concentrations of each of the three peptides were used, *i.e.*, 1.667 μM, 5.0 μM, and 15.0 μM. In positive control experiments, 0.05% Triton X-100 was added to the vesicles, resulting in complete rupture of the vesicles. In negative control experiments, plane DPC micelles or blank buffer was added. The buffer resulted in no increase in fluorescence, and the effect of DPC without the peptide was <5% of that generated by the peptides. Before and after fluorescence

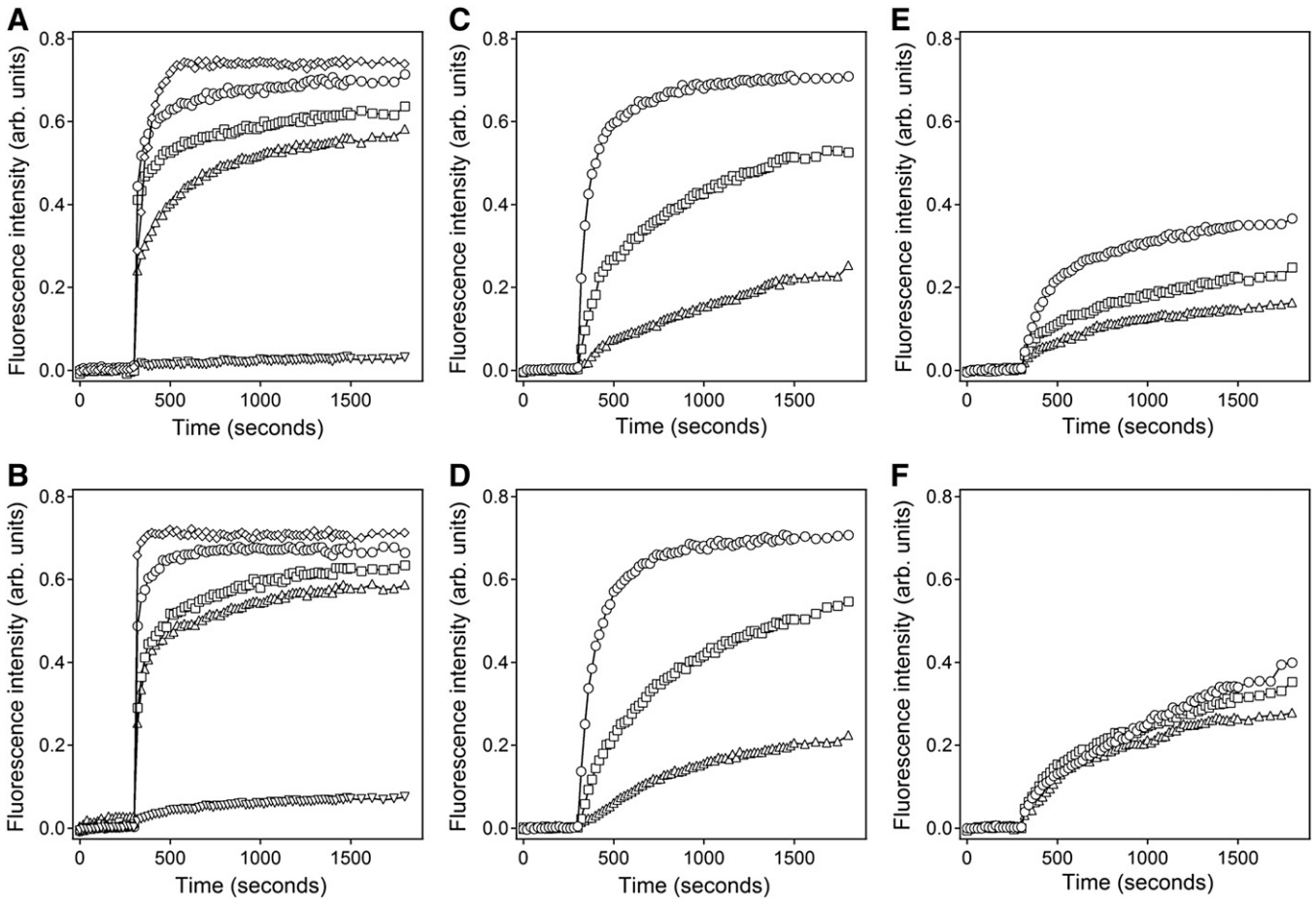

Fig. 2. Peptides cause efficient calcein release from vesicles. Kinetics of peptide-induced calcein release from phospholipid vesicles composed of 100% POPC (A, C, E) or POPC/POPG at a 7:3 molar ratio (B, D, F). The peptides BaxC-KK (A, B), BaxC-EE (C, D) and BaxC-LL (E, F) were added to 10 mM calcein-loaded vesicles at 300 s at concentrations 1.667 μM (triangles), 5.0 μM (squares), or 15.0 μM (circles). Inverted triangles and rhombs in panels A and B indicate the effects of plane DPC and Triton X-100 at final concentrations of 0.6 mM and 0.05%, respectively. Temperature, buffer, and other experimental conditions were as in Fig. 1.

measurements, right angle light scattering of the sample was measured at 550 nm to determine if vesicle integrity was affected by the peptides, DPC, or Triton X-100.

3. Results and discussion

3.1. Membrane permeabilization by peptides

The C-terminal helix 9 of Bax is in a hydrophobic groove of the protein, with the side chains of the two lysines oriented outward (Fig. S1A of Supplementary data). Hydropathy analysis of Bax sequence using MPEx [33] indicated that the C-terminal helix 9 had a substantial hydropathy index and hence a strong propensity to form a transmembrane conformation that might mediate membrane pore formation (Fig. S1B).

Membrane permeabilization by the peptides was studied by monitoring peptide-induced calcein release from lipid vesicles. Calcein fluorescence is self-quenched at concentrations higher than ~1 mM [32,34–36]. This results in a bell-shaped curve of the concentration-dependence of calcein fluorescence, as shown in Fig. 1A. If lipid vesicles are loaded with calcein at a relatively high concentration, then membrane permeabilization can be detected by calcein release into the large external compartment, resulting in calcein dilution, dequenching, and increase in fluorescence intensity. We used lipid vesicles 200 nm in diameter at 0.5 mM total lipid concentration loaded with 10 mM calcein. Using 4.0 nm for POPC or POPC/POPG membrane thickness [37] and 0.68 nm^2 for cross-sectional area per lipid [38], one can evaluate a 0.31% fraction of vesicle-entrapped volume. Upon total disruption of the vesicles, calcein concentration in the external volume will increase from zero to ~0.03 mM, which corresponds to an increase in fluorescence intensity to 1.0–1.1 relative units, as judged from data of Fig. 1A. Fig. 1B shows the representative fluorescence spectra indicating a rapid increase in calcein fluorescence intensity upon addition of 1.667 μM of BaxC-KK to calcein-loaded vesicles. To ensure that calcein release from the vesicles was due to membrane pore formation rather than vesicle rupture, vesicle integrity was estimated by right angle light scattering on a J-810 spectrofluoropolarimeter. When incident light was used at 550 nm, slightly red-shifted light scattering from vesicles was detected (Fig. 1C). Addition of 1/10th volume of buffer resulted in a ~10% decrease in intensity of scattered light due to dilution of the vesicle suspension. Addition of 1/10th volume of plane DPC (at final DPC concentration of 0.6 mM) or any of the three peptides solubilized in DPC at final peptide concentration of 1.667 μM to15 μM did not result in any additional decrease in light scattering, indicating that neither the peptides nor DPC below its cmc of 1.5 mM caused vesicle disruption. However, the possibility that pore formation by the peptides is accompanied with membrane destabilization cannot be ruled out. Triton X-100 caused strong reduction of light scattering. The residual scattering was due to mixed Triton X-100-lipid micelles, indicating complete degradation of the vesicles by Triton X-100.

To exclude the possibility that the observed effect of calcein release could result from a nonspecific action of peptide–DPC complex on the vesicles, additional experiments have been conducted where two different peptides have been solubilized in DPC micelles and added to calcein-loaded vesicles. An amphipathic peptide corresponding to N-terminus of human group IB phospholipase A_2, named IB, and a hydrophobic peptide corresponding to the C-terminal "transmembrane" domain of Bcl-x_L, named XL, were tested. As shown in Fig. S2A, B, addition of empty DPC micelles to calcein-loaded POPC or POPC/POPG (7:3) vesicles caused a mall reduction of calcein fluorescence, reflecting sample dilution and hence indicating practically zero effect of DPC. Addition of DPC micelles containing the IB peptide to POPC vesicles did not elicit any appreciable calcein release (Fig. S2C), and caused a slight effect of calcein release in case of anionic POPC/POPG vesicles (Fig. S2D). Addition of DPC micelles containing the XL peptide exerted a moderate effect on POPC vesicles but caused a strong time-dependent calcein release from POPC/POPG vesicles (Fig. S2E, F). These data clearly indicate that a) DPC itself does not cause membrane permeabilization, b) the IB peptide, which is known to bind to phospholipid membranes peripherally [31] exerts little permeabilizing effect on membranes, and c) the Bcl-x_L peptide, which is known to insert in artificial and biological membranes and cause membrane leakage [39] efficiently permeabilizes the membranes. Hence, calcein release directly correlates with the intrinsic membranotropic properties of the peptides.

3.2. Kinetics and mechanism of pore formation

Addition of the peptides to calcein-loaded vesicles resulted in a gradual increase in calcein fluorescence, apparently induced by membrane permeabilization by the peptides and calcein release (Fig. 2). While the

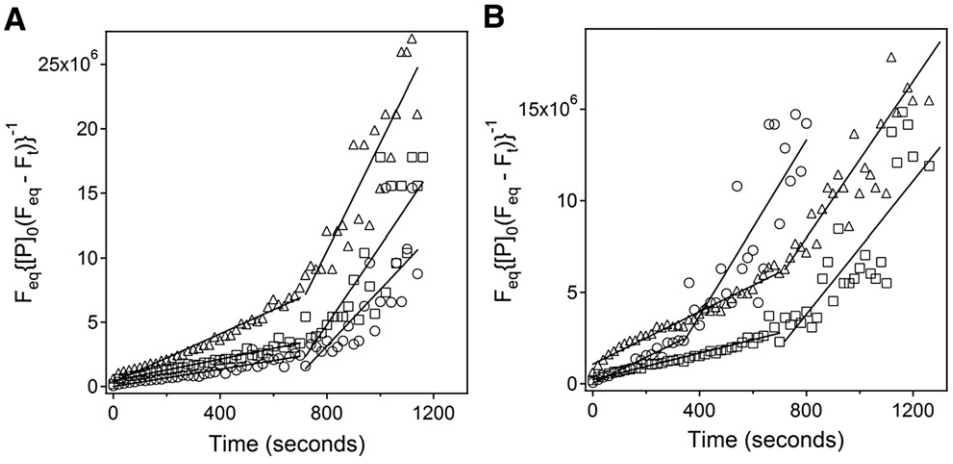

Fig. 3. Pore formation by BaxC-KK peptide is a biphasic process. Time-dependence of vesicle content release is presented using a second-order reaction formalism for pore formation by the peptides (see Eq. (3)). Panels A and B correspond to vesicles composed of pure POPC and POPC/POPG at a 7:3 molar ratio, respectively. Triangles, squares, and circles correspond to BaxC-KK peptide concentrations of 1.667 μM, 5.0 μM, and 15.0 μM, respectively. The slope of the graphs indicates the second-order rate constant of peptide–peptide interactions in the membrane, leading to pore formation.

Table 1
Kinetic parameters of calcein release from vesicles composed of 100% POPC (PC) or 70% POPC + 30% POPG (PC/PG) derived from fitting the data with a double-exponential equation: $F_t = F_{eq} - a_1\exp(-k_1 t) - a_2\exp(-k_2 t)$, where F_t is calcein fluorescence intensity at time t, F_{eq} is F_t at $t \to \infty$, k_1 and k_2 are the rate constants. C_p is the peptide concentration in μM.

C_p	F_{eq}		a_1		a_2		k_1 (s^{-1})		k_2 (s^{-1})	
	PC	PC/PG	PC	PC/PG	PC	PC/PG	PC	PC/PG	PC	PC/PG
BaxC-KK										
1.667	0.5622	0.5969	0.2974	0.1917	0.2633	0.3724	0.002939	0.001936	0.086286	0.038464
5.0	0.6224	0.6312	0.1722	0.2236	0.4508	0.3949	0.002589	0.002632	0.105304	0.050731
15.0	0.6920	0.6726	0.1555	0.1618	0.5283	0.5078	0.0035407	0.005551	0.074997	0.115064
BaxC-EE										
1.667	0.3811	0.2555	0.1652	0.1175	0.2008	0.1387	0.001164	0.000817	0.000401	0.002029
5.0	0.5912	0.6078	0.4165	0.4592	0.1784	0.1529	0.001362	0.001256	0.015592	0.008628
15.0	0.7075	0.7020	0.2238	0.2382	0.4733	0.4596	0.003443	0.003539	0.025874	0.015385
BaxC-LL										
1.667	0.2076	0.3264	0.1244	0.2412	0.07143	0.0784	0.000629	0.001130	0.004593	0.007391
5.0	0.2781	0.5085	0.2002	0.3918	0.07003	0.1085	0.001035	0.000573	0.017925	0.011937
15.0	0.3969	0.6134	0.1933	0.2302	0.2013	0.3390	0.001136	0.001239	0.010174	0.000376

kinetics and the level of calcein release were dependent upon the type and the concentration of the peptide and the lipid composition of vesicle membranes, all kinetic curves demonstrated a double-exponential character, as shown in Fig. S3. All traces of time-dependence of calcein fluorescence could be fitted with $F_t = F_{eq} - a_1\exp(-k_1 t) - a_2\exp(-k_2 t)$, where F_t is the calcein fluorescence intensity at time t, offset by subtraction of the fluorescence before peptide addition, F_{eq} is the extrapolated level of fluorescence at $t \to \infty$, a_1 and a_2 are the fractions of the two kinetic components, and k_1 and k_2 are the respective rate constants. The time constants of the fast and slow components were within the range of 0.2–1.5 min and 3–30 min, respectively, depending on the peptide type and concentration and the membrane charge (Table 1).

Upon membrane binding of the peptides and pore formation, the observed calcein fluorescence increases and reaches an equilibrium

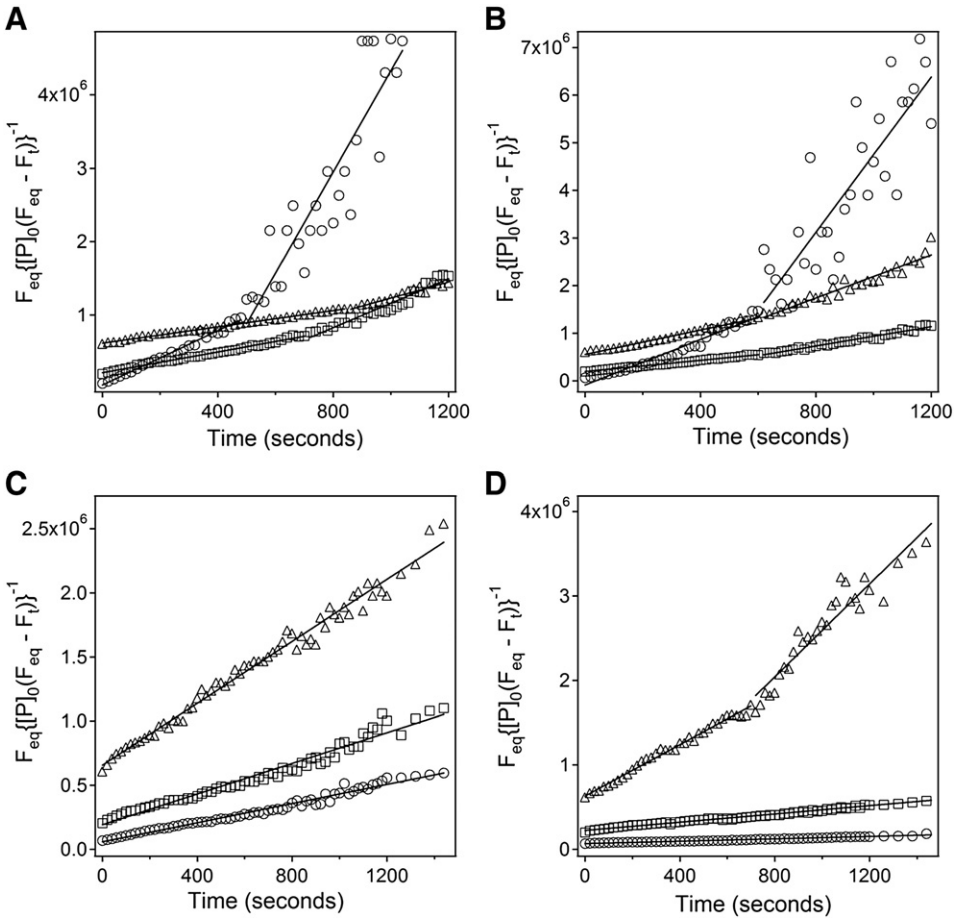

Fig. 4. Pore formation by BaxC-EE and BaxC-LL peptides tends to be a monophasic process. Description of time-dependence of vesicle content release using a second-order reaction formalism for pore formation by peptides BaxC-EE (A, B) and BaxC-LL (C, D) in membranes of 100% POPC (A, C) or 70% POPC + 30% POPG (B, D) membranes. Triangles, squares, and circles correspond to peptide concentrations of 1.667 μM, 5.0 μM, and 15.0 μM, respectively. The slope of the graphs indicates the second-order rate constant of peptide–peptide interactions.

value, F_{eq}. If all peptide molecules participate in pore formation, then the concentration of free peptide at time t, $[P]_t$, can be expressed through the total peptide concentration, $[P]_0$, and fluorescence intensity at time t, F_t, as follows:

$$[P]_t = [P]_0\left(1-\frac{F_t}{F_{eq}}\right). \quad (1)$$

Given the hydrophobic nature of the peptides and their poor water solubility, it is reasonable to assume that nearly all of the peptide ends up in vesicle membranes upon dispersion of DPC. We use a model of pore formation where peptide molecules associate with each other in a stepwise fashion to form an oligomeric assembly [34,40–42]. If the pore is composed of $n \geq 2$ peptide molecules, then addition of each monomer to the assembly can be considered a second-order process that is described as follows [43]:

$$\frac{1}{[P]_t}-\frac{1}{[P]_0} = k_a t \quad (2)$$

where k_a is the second-order rate constant in units $M^{-1}\ s^{-1}$. Combination of Eqs. (1) and (2) yields:

$$\frac{F_{eq}}{[P]_0\left(F_{eq}-F_t\right)} = \frac{1}{[P]_0} + k_a t. \quad (3)$$

Eq. (3) indicates that the second-order rate constant of pore formation, k_a, can be determined as the slope of the time dependence of the term at the left-hand side of Eq. (3). Values of $F_{eq}/\{[P]_0(F_{eq}-F_t)\}$ were calculated using F_t and F_{eq} from the experimental kinetic curves shown in Fig. 2 and Fig. S3 and were plotted *vs.* time. (Values of F_{eq} are tabulated in Table 1.) Data of Fig. 3 indicate an initial linear time dependence of $F_{eq}/\{[P]_0(F_{eq}-F_t)\}$, characteristic of a bimolecular reaction, followed by a second segment of linear dependence with a higher slope at $t \geq 10$ min after addition of the wild-type BaxC-KK peptide to calcein-loaded vesicles (for POPC/POPG vesicles and 15 μM peptide, the second linear segments start earlier). The data points corresponding to the second linear segment are considerably scattered because with increasing time F_t approaches F_{eq} and the values of $F_{eq}/\{[P]_0(F_{eq}-F_t)\}$ become progressively unstable as the denominator approaches zero.

Generally, a bimolecular process where reactants A and B combine in a complex AB, which then either dissociates to A and B or leads to the formation of the final product P, can be described as shown in Scheme 1 [43]:

$$A + B \rightleftharpoons_{k_d}^{k_a} AB \xrightarrow{k_p} P. \quad \text{Scheme1}$$

Here, k_a and k_d are the forward and reverse rate constants of complex formation, and k_p is the rate constant of product formation. The effective (observed) rate constant of product formation is

$$k_{eff} = \frac{k_a k_p}{k_p + k_d}. \quad (4)$$

Two cases can be considered. First, product formation is much faster than complex dissociation ($k_p \gg k_d$). This leads to:

$$k_{eff} \approx k_a. \quad (5)$$

Second, complex dissociation is much faster than product formation ($k_p \ll k_d$). This leads to:

$$k_{eff} \approx \frac{k_a k_p}{k_d} = K k_p. \quad (6)$$

Here, $K = k_a/k_d$ is the peptide–peptide association (affinity) constant in units M^{-1}.

Two linear segments of the graphs shown in Fig. 3 indicate that at least two processes are involved in membrane pore formation. The first question to be answered is whether any of the two processes are related to diffusion of the peptide molecules in the membrane. The second-order rate constant of a diffusion-controlled bimolecular process is [43]: $k_{diff} = 4\pi RDN_A$, where R is the distance of closest approach between the two reactants, D is the sum of diffusion coefficients of the two reactants, and N_A is Avogadro's number. The diffusion coefficients of lipid or peptide molecules in fluid lipid membranes are in the range 1×10^{-8} to 1×10^{-7} cm^2/s^{-1} [44]. The distance of interaction of two peptides in α-helical or β-strand conformations is ~1.0 or ~0.5 nm, respectively [45,46]. With these considerations, we estimate $k_{diff} = 8\times10^6$ to 1.5×10^8 $M^{-1}\ s^{-1}$. The rate constants k_{a1} and k_{a2} shown in Table 2 are at least 10^3-fold smaller than the estimated value of k_{diff}, indicating that the pore formation is much slower than a simple diffusion-controlled process. This in turn implies that in most cases peptides can diffuse away from each other before the complex is formed. Thus, the rate constant of peptide

Table 2
The fraction of maximum possible vesicle content leakage (F_{rel}), second-order rate constants (k_{a1} and k_{a2}), and peptide–peptide affinity constants (K_1 and K_2) characterizing membrane pore formation by the peptides. Parameters k_{a1} and K_1 were derived from the data for initial time period (up to 10 min) following addition of peptides to the vesicles, while k_{a2} and K_2 were derived from data corresponding to later times (between 10 and 20 min). C_p is the peptide concentration in μM.

C_p	F_{rel}		k_{a1} ($M^{-1}\ s^{-1}$)		k_{a2} ($M^{-1}\ s^{-1}$)		K_1 (M^{-1})		K_2 (M^{-1})	
	PC	PC/PG	PC	PC/PG	PC	PC/PG	PC	PC/PG	PC	PC/PG
BaxC-KK										
1.667	0.755	0.843	8966	7190	41,800	21,407	3.05×10^6	3.71×10^6	1.42×10^7	1.11×10^7
5.0	0.836	0.892	4459	4608	34,090	19,538	1.72×10^6	1.75×10^6	1.31×10^7	7.42×10^6
15.0	0.929	0.950	4871	7318	21,973	26,868	1.37×10^6	7.71×10^5	6.21×10^6	4.84×10^6
BaxC-EE										
1.667	0.513	0.332	552	1276	1092	2267	4.74×10^5	1.56×10^6	9.38×10^5	2.77×10^6
5.0	0.796	0.789	710	594	1672	1010	5.21×10^5	4.73×10^5	1.23×10^6	8.04×10^5
15.0	0.952	0.912	1852	2389	6892	8156	5.38×10^5	6.75×10^5	2.00×10^6	2.30×10^6
BaxC-LL										
1.667	0.317	0.407	1208	1526	–	2748	1.92×10^6	1.35×10^6	–	2.43×10^6
5.0	0.425	0.634	598	243	–	–	5.77×10^5	4.24×10^5	–	–
15.0	0.606	0.765	373	70	–	–	3.28×10^5	1.87×10^5	–	–

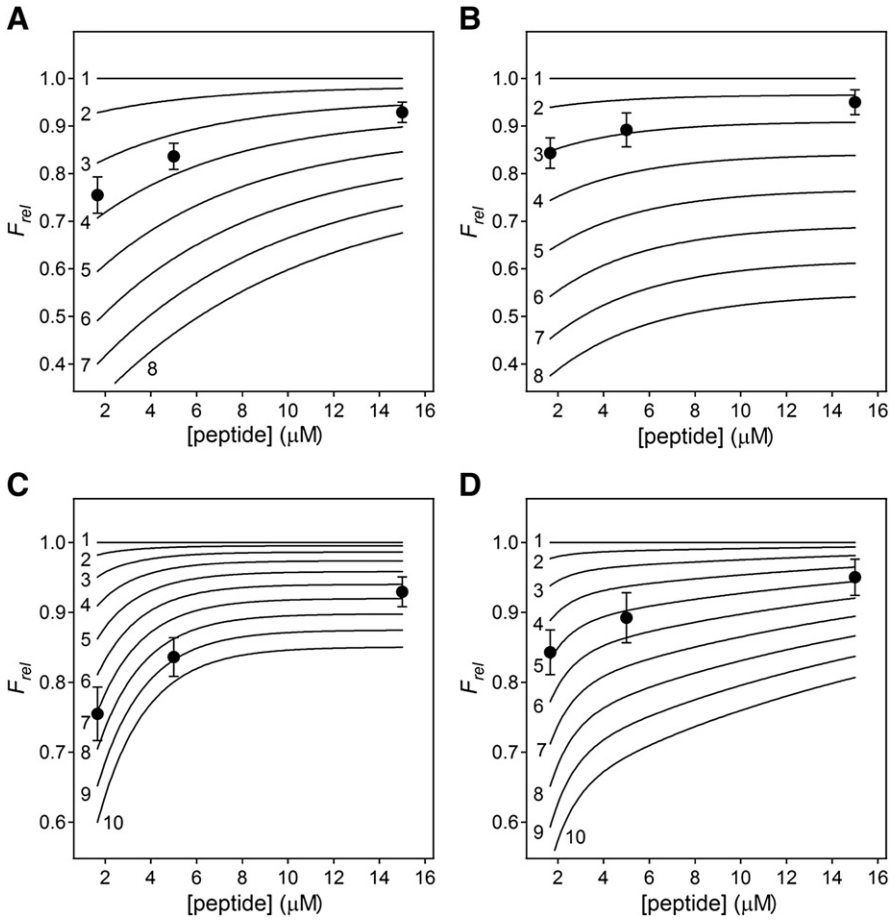

Fig. 5. BaxC-KK pores contain 3–4 molecules in the nucleation complex and up to 8 molecules in the mature pore. Dependence of the fraction of vesicle content leakage relative the maximum leakage (F_{rel}) on the concentration of BaxC-KK peptide. Experimental data at three peptide concentrations are presented along with curves simulated according to a reversible aggregation model (Eq. (9)), using various numbers of peptide molecules involved in pore formation, as indicated at the left hand side of the curves. Panels A and C correspond to POPC vesicles, and panels B and D to POPC/POPG (7:3) vesicles. Curves shown in panels A and B are simulated using the rate constant, k_a, for earlier times following peptide addition, *i.e.* corresponding to the first linear segments of traces shown in Fig. 3. Curves shown in panels C and D are simulated using the rate constant, k_a, for later times following peptide addition, *i.e.* corresponding to the second linear segments of traces shown in Fig. 3. All curves are simulated using the slow components of double exponential rate constants summarized in Table 1.

complex formation, k_p, is the rate-determining step, and therefore, according to Eq. (6), $k_{eff} = Kk_p$. Here, k_{eff} is the observed second-order rate constant, *i.e.* those summarized in Table 2 as k_{a1} and k_{a2}, K is the peptide–peptide association constant, and k_p is the rate constant of peptide complex formation. Since vesicle content leakage results from peptide complex formation in the membrane, one of the double-exponential rate constants that describe the observed kinetics of calcein release can be used for k_p. Peptide–peptide binding constants evaluated using both k_{a1} and k_{a2}, which describe the experimental data at earlier and later time periods following peptide addition, in combination with the rate constant corresponding to the slow component of double-exponential time course are presented in Table 2 as K_1 and K_2. Binding constants have also been evaluated using the rate constants corresponding to the fast component of double-exponential time course, but these values were far beyond the experimental observations and therefore have been discarded (see below).

Analysis of the kinetic data on vesicle content leakage induced by BaxC-KK indicates two distinct processes with rate constants of 5000–9000 $M^{-1}\,s^{-1}$ and 20,000–40,000 $M^{-1}\,s^{-1}$ (Table 2). The slower process likely reflects the nucleation of the pore complex, which is the rate-limiting step of pore formation and is characterized with peptide–peptide affinity constants of $K_1 = (0.8–3.7)\times10^6\ M^{-1}$. The second process is interpreted in terms of formation of the final pore structure, which proceeds at a 4-fold higher speed and results in peptide–peptide association with affinity constants of $K_2 = (0.5–1.4)\times10^7\ M^{-1}$.

Similar analysis of data for BaxC-EE and BaxC-LL mutant peptides indicated distinct features of membrane pore formation by these molecules. BaxC-EE showed a strong biphasic feature of the time course of pore formation only for the highest peptide concentration of 15 μM (Fig. 4A, B). The peptide–peptide affinity constants corresponding to the initial and later phases of pore formation were approximately an order of magnitude lower than those of the wild-type BaxC-KK peptide (Table 2). BaxC-LL peptide displayed a linear time course of pore formation, except for POPC/POPG membranes at the lowest concentration of 1.667 μM (Fig. 4C, D). The peptide–peptide affinity constants characterizing these monophasic processes of complex formation were $(0.2–2.0)\times10^6\ M^{-1}$ (Table 2), *i.e.* comparable to those for the wild type peptide at initial times. However, the larger slope of the second phase of time dependence of pore formation by BaxC-LL in POPC/POPG membranes (Fig. 4D, triangles) yielded a larger affinity constant of $2.4\times10^6\ M^{-1}$. Thus, pore formation by the mutant peptides tends to be a monophasic process, especially in case of the most hydrophobic peptide BaxC-LL. The peptide–peptide affinity constants involved in the initial pore nucleation are in the range $(0.1–3.7)\times10^6\ M^{-1}$ and those involved in the formation of the more stable pore structure are $(0.8–14)\times10^6\ M^{-1}$. These

correspond to Gibbs free energies of −10 to −12 kcal/mol and −11 to −13 kcal/mol, respectively. Considering that the strength of peptide hydrogen bonding is close to −1.5 kcal/mol [47,48], these peptide–peptide binding energies are equivalent to up to 8 hydrogen bonds and should be viewed as strong enough to sustain an oligomeric pore structure.

3.3. The oligomeric state of the pore

The number of peptide monomers per pore can be estimated using a formalism of reversible aggregation [34,40,41]. This model is applicable to general cases when the sample contains $j=1$ to S different types of vesicles, such as vesicles of different size categories, and each vesicle of type j contains up to N_j peptide molecules. If the number of peptides per pore is n, then leakage will be observed when the number of peptides per vesicle i is in the range $n \le i \le Nj$. The fraction of leakage reached at $t \to \infty$ (F_{eq}, see above) relative to the maximum possible leakage (F_{max}) caused by vesicle rupture by Triton X-100, is given as:

$$F_{rel} = \frac{F_{eq}}{F_{max}} = \left[q^{n-1}(n - nq + q)\right] \sum_{i=n}^{N_j} \sum_{j=1}^{S} A_{i,j} f_j \tag{7}$$

where

$$q = \frac{1}{\alpha + \sqrt{\alpha^2 - 1}} \tag{7a}$$

$$\alpha = 1 + \frac{1}{4K[P]_0}. \tag{7b}$$

In Eq. (7), $A_{i,j}$ is the normalized fraction of vesicles of size j that contain i bound peptides, and f_j is the fraction of encapsulated volume of vesicles of type j normalized relative to the total encapsulated volume. Considering that the vesicles used in this work have been obtained by extrusion through filters of defined pore size (200 nm), only one type of vesicles can be considered, *i.e.*, $S=1$. Furthermore, it is reasonable to assume that all vesicles contain similar numbers of peptides, *i.e.* the average number of peptide molecules per vesicle. Under our experimental conditions (total lipid concentration of 0.5 mM and peptide concentrations of 1.667 μM, 5.0 μM, and 15.0 μM), this number varied between 1,180 and 10,650, which is much larger than any conceivable number of peptide molecules per pore. With these considerations, we arrive at

$$\sum_{j=1}^{S} f_j = 1 \quad \text{and} \quad \sum_{i=n}^{N_j} A_{i,j} = 1. \tag{8}$$

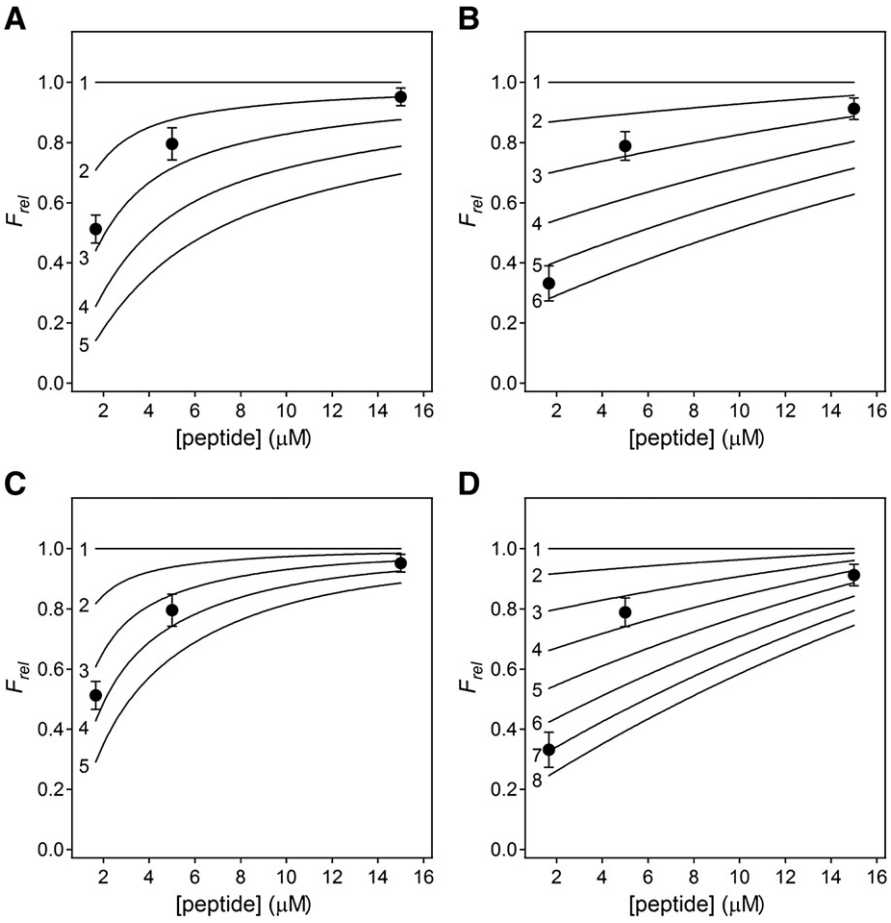

Fig. 6. BaxC-EE pores contain up to 6–8 peptide molecules. Dependence of the fraction of vesicle content leakage relative the maximum leakage (F_{rel}) on the concentration of BaxC-EE peptide. Experimental data at three peptide concentrations are presented along with curves simulated according to a reversible aggregation model (Eq. (9)), using various numbers of peptide molecules involved in pore formation, as indicated at the left hand side of the curves. Panels A and C correspond to POPC vesicles, and panels B and D to POPC/POPG (7:3) vesicles. Curves shown in panels A and B are simulated using the rate constant, k_a, for earlier times following peptide addition, *i.e.* corresponding to the first linear segments of traces shown in Fig. 4A, B. Curves shown in panels C and D are simulated using the rate constant, k_a, for later times following peptide addition, *i.e.* corresponding to the second linear segments of traces shown in Fig. 4A, B. All curves are simulated using the slow components of double exponential rate constants summarized in Table 1.

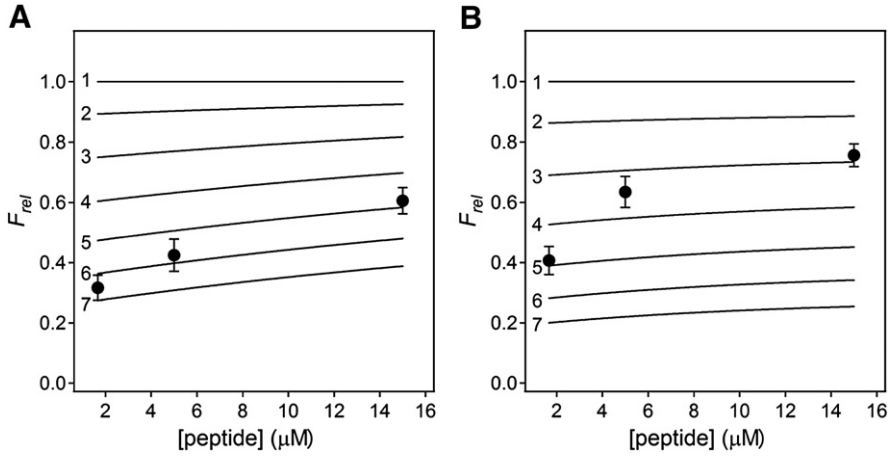

Fig. 7. BaxC-LL pores contain up to 5–7 peptide molecules. Dependence of the fraction of vesicle content leakage relative the maximum leakage (F_{rel}) on the concentration of BaxC-LL peptide. Experimental data at three peptide concentrations are presented along with curves simulated according to a reversible aggregation model (Eq. (9)), using various numbers of peptide molecules involved in pore formation, as indicated at the left hand side of the curves. Panels A and B correspond to POPC and POPC/POPG (7:3) vesicles, respectively. Curves are simulated using the rate constant, k_a, deduced from the linear traces shown in Fig. 4C, D (for POPC/POPG membranes at 1.667 μM peptide concentration, the value of k_a corresponding to the initial time domain is used.) All curves are simulated using the slow components of double exponential rate constants summarized in Table 1.

Combination of Eqs. (7) and (8) yields:

$$F_{rel} = q^{n-1}(n - nq + q). \quad (9)$$

If experiments of vesicle content release are performed at various peptide concentrations, then the experimental values of F_{rel} can be determined at each concentration and compared with those calculated through Eq. (9) using different values for n. Values of n at which the calculated and measured values of F_{rel} merge will indicate the number of peptide molecules per pore. It should be noted that this procedure of determination of n is more accurate than a model considering an irreversible aggregation, in which overestimated values of n are obtained [42].

Experimental values of relative leakage, $F_{rel} = F_{eq}/F_{max}$, were determined for each peptide concentration for both POPC and POPC/POPG membranes and plotted *vs.* peptide concentration. Values of F_{rel} were then calculated through Eq. (9) using various numbers of peptide molecules per pore (parameter n in Eq. (9)) and plotted *vs.* peptide concentration. The number of peptide molecules in the pore structure was found as the parameter n at which an agreement was reached between the theoretical and experimental data. Calculations of F_{rel} involved the peptide–peptide affinity constant $K = k_{eff}/k_p$, where k_{eff} and k_p are the second-order rate constant in units $M^{-1}\,s^{-1}$ derived from the graphs of Figs. 3 and 4 and the observed rate constant of vesicle leakage in units s^{-1} given by the double-exponential curves shown in Fig. S3. Since we have two values for k_{eff} and two for k_p, total four plots have been constructed for each peptide-membrane pair. As shown in Fig. S4, the data could be described by the curves simulated using the slow double-exponential component, while the theoretical curves obtained using the fast component of the double-exponential time course (dashed lines) were far off the range of experimental data. Therefore, the mechanism of pore formation was analyzed using the slower double-exponential rate constants, which apparently reflect the kinetics of pore formation.

Fig. 5 indicates that when values of k_{a1} are used, which characterize the pore formation process at earlier times (5–10 min), the experimental data for BaxC-KK agree with $n \approx 3$–4 for POPC membranes (Fig. 5A) and $n \approx 2$–3 for POPC/POPG membranes (Fig. 5B). When values of k_{a2} are used, which characterize further progression of pore formation process, the data are consistent with $n \approx 8$ for POPC membranes (Fig. 5C) and $n \approx 5$ for POPC/POPG membranes (Fig. 5D). Thus, the overall picture of membrane pore formation by the wild-type BaxC-KK peptide is that the peptide molecules form an initial nucleation complex, which involves 2–4 molecules and is characterized with affinity constants of $(0.8–3.7)\times10^6\ M^{-1}$, followed by a more efficient process (higher 2nd order rate constant) of the assembly of the final pore structure involving up to 8 peptide molecules associated with affinity constants of $(0.5–1.4)\times10^7\ M^{-1}$.

Evaluation of the oligomeric state of the pores formed by BaxC-EE was consistent with 2–3 peptide molecules in the nucleation complex that increased with time to a larger number (3–4 for POPC and 4–7 for POPC/POPG membranes) (Fig. 6). The number of BaxC-LL peptide molecules in the pore complex was estimated to be 5–7 for POPC membranes and 3–5 for POPC–POPG membranes (Fig. 7). However, data corresponding to the second phase of pore formation in POPC/POPG membranes by 1.667 μM BaxC-LL peptide (Fig. 4D, triangles) indicate $n = 6$–7 molecules in the pore complex.

Although membrane pore formation has been demonstrated for Bax helices 5, 6, and 9, [28,29,49,50], molecular details such as the oligomeric state of the pore, the kinetic and peptide–peptide affinity parameters have not been reported. Our data indicate up to eight peptide molecules assemble within the membrane, stabilized by affinity constants of 10^6–$10^7\ M^{-1}$, and form membrane pores that efficiently transport calcein molecules. Peptide-induced release of calcein from lipid vesicles indicates the pores are quite large, at least 13 Å in diameter, as the hydrodynamic radius of calcein is 6.4 Å [51]. Numbers of pore-forming peptide units in the pore between 3 and 10 have been reported [35,41,42,52–56]. While our data are consistent with a maximum of eight peptide molecules in the pore structure, formation of pores with a lower oligomeric state cannot be ruled out. The oligomeric state of the pore may depend on factors like the membrane surface charge and the peptide sequence, as shown, for example, for melittin [35] and the GALA peptide [57]. The efficiency of pore formation by the wild-type BaxC-KK peptide, as judged from the second-order rate constants and affinity constants summarized in Table 2, is by an order of magnitude greater as compared to the BaxC-EE and BaxC-LL mutants. However, no clear correlation was detected between pore formation and the membrane surface charge. Also, the kinetic and affinity constant for the cationic BaxC-KK pore formation in anionic membranes exceeded those of the anionic BaxC-EE peptide less than 10-fold (Table 2). The fact that the wild-type and mutant Bax peptides, which significantly differ in their charge, form pores in both zwitterionic and anionic membranes with only slight differences indicates that the peptides use the "barrel-stave" rather than the "carpet" mechanism, *i.e.*, the hydrophobic peptide–membrane interactions dominate over electrostatic interactions [58].

Data of this study provide new insight into the mechanism of membrane pore formation by Bax C-terminal peptide. As confirmed by our tryptophan fluorescence quenching data (not shown), the peptide significantly inserts into the membrane hydrophobic core, consistent with the barrel-stave mechanism. The second-order rate constants of pore nucleation and assembly of the mature pore indicate that pore formation is slower, and hence more complex, than a simple diffusion-controlled process. Interactions between the peptide monomers within the membrane are evidently followed by formation of a specific structure, leading to the final pore architecture that is supported by high-affinity (−10 to −13 kcal/mol) peptide–peptide interactions. Our attenuated total reflection Fourier transform infrared studies indicate that the peptide molecules include α-helical and β-strand secondary structures, both of which are tilted relative to the membrane normal (unpublished data). Infrared data were obtained on stacked lipid–peptide films on a germanium plate under conditions where the film thickness significantly exceeded the evanescent wave decay length, so only the membrane-inserted peptide molecules could contribute to the spectra. Altogether, the C-terminal 20-residue peptide of Bax emerges as a potent cytotoxic agent that is able to form transmembrane pores containing up to eight monomers and at least 13 Å in diameter. Further analysis of the structural basis of membrane pore formation will allow development of novel cytotoxic peptides.

4. Conclusions

Bax is known to bind to the mitochondrial membrane and directly mediate cytochrome *c* release, supposedly by a pore forming mechanism. The C-terminal peptide of Bax alone was shown to permeabilize lipid membranes. Moreover, our recent data indicated that the peptide, when delivered *via* polymer-based nanoparticles, has a strong cytotoxic potency against breast and colon cancer cells in mice [30]. Thus, the peptide corresponding to Bax C-terminus emerges as an attractive molecular tool for development of cytotoxic therapeutics, which will require a better understanding of its membrane pore formation mechanism. This work clearly demonstrates that the C-terminal 20-residue stretch of Bax has the capability of forming relatively large membrane pores with a radius of at least 13 Å. Replacement of the two lysine residues close to the C-terminus with anionic glutamate or nonpolar leucine residues reduces the pore forming activity of the peptide, consistent with the lethal effects of the peptides on cancer cells. Data on calcein release kinetics at various peptide concentrations allow determination of the second-order rate constants of pore formation, the intermolecular affinities of peptide molecules within the pore, and the oligomeric state of the pore. In general, the pore formation is a two-stage process, nucleation and assembly of the final pore structure that includes up to eight peptide molecules and is stabilized by intermolecular interaction energies of −10 to −13 kcal/mol. The pore forming activities of the peptides can be exploited for therapeutic purposes. For example, the membrane pore forming activity of Bax helix 5 has been used to cause caspase-dependent cell death and tumor regression in mice [5]. Thus, the importance of our findings is two-fold. First, the potent membrane pore forming activity of Bax C-terminus accentuates its potential role in membrane permeabilization by Bax. Second, based on our data, cytotoxic peptide-based molecular tools can be developed for cell membrane perforation and killing of unwanted cells such as bacteria, fungi, or cancer cells.

Acknowledgements

Financial support from the National Institutes of Health grant GM083324 is gratefully acknowledged.

Appendix A. Supplementary data

Supplementary data to this article can be found online at http://dx.doi.org/10.1016/j.bbamem.2012.08.006.

References

[1] A. Antignani, R.J. Youle, How do Bax and Bak lead to permeabilization of the outer mitochondrial membrane? Curr. Opin. Cell Biol. 18 (2006) 685–689.
[2] B. Leber, J. Lin, D.W. Andrews, Embedded together: the life and death consequences of interaction of the Bcl-2 family with membranes, Apoptosis 12 (2007) 897–911.
[3] R.J. Youle, A. Strasser, The BCL-2 protein family: opposing activities that mediate cell death, Nat. Rev. Mol. Cell Biol. 9 (2008) 47–59.
[4] S.W. Tait, D.R. Green, Mitochondria and cell death: outer membrane permeabilization and beyond, Nat. Rev. Mol. Cell Biol. 11 (2010) 621–632.
[5] J.G. Valero, L. Sancey, J. Kucharczak, Y. Guillemin, D. Gimenez, J. Prudent, G. Gillet, J. Salgado, J.L. Coll, A. Aouacheria, Bax-derived membrane-active peptides act as potent and direct inducers of apoptosis in cancer cells, J. Cell Sci. 124 (2011) 556–564.
[6] B. Antonsson, S. Montessuit, B. Sanchez, J.C. Martinou, Bax is present as a high molecular weight oligomer/complex in the mitochondrial membrane of apoptotic cells, J. Biol. Chem. 276 (2001) 11615–11623.
[7] X. Roucou, S. Montessuit, B. Antonsson, J.C. Martinou, Bax oligomerization in mitochondrial membranes requires tBid (caspase-8-cleaved Bid) and a mitochondrial protein, Biochem. J. 368 (2002) 915–921.
[8] J.D. Robertson, B. Zhivotovsky, V. Gogvadze, S. Orrenius, Outer mitochondrial membrane permeabilization: an open-and-shut case? Cell Death Differ. 10 (2003) 485–487.
[9] L. Zhou, D.C. Chang, Dynamics and structure of the Bax–Bak complex responsible for releasing mitochondrial proteins during apoptosis, J. Cell Sci. 121 (2008) 2186–2196.
[10] A.J. Garcia-Sáez, G. Fuertes, J. Suckale, J. Salgado, Permeabilization of the outer mitochondrial membrane by Bcl-2 proteins, Adv. Exp. Med. Biol. 677 (2010) 91–105.
[11] L. Ghibelli, M. Diederich, Multistep and multitask Bax activation, Mitochondrion 10 (2010) 604–613.
[12] D. Westphal, G. Dewson, P.E. Czabotar, R.M. Kluck, Molecular biology of Bax and Bak activation and action, Biochim. Biophys. Acta 1813 (2011) 521–531.
[13] T. Brustovetsky, T. Li, Y. Yang, J.T. Zhang, B. Antonsson, N. Brustovetsky, BAX insertion, oligomerization, and outer membrane permeabilization in brain mitochondria: role of permeability transition and SH-redox regulation, Biochim. Biophys. Acta 1797 (2010) 1795–1806.
[14] R.F. Epand, J.C. Martinou, S. Montessuit, R.M. Epand, C.M. Yip, Direct evidence for membrane pore formation by the apoptotic protein Bax, Biochem. Biophys. Res. Commun. 298 (2002) 744–749.
[15] Y. Lazebnik, Why do regulators of apoptosis look like bacterial toxins? Curr. Biol. 11 (2001) R767–R768.
[16] P.H. Schlesinger, M. Saito, The Bax pore in liposomes, Biophys. Cell Death Differ. 13 (2006) 1403–1408.
[17] B. Antonsson, F. Conti, A. Ciavatta, S. Montessuit, S. Lewis, I. Martinou, L. Bernasconi, A. Bernard, J.J. Mermod, G. Mazzei, K. Maundrell, F. Gambale, R. Sadoul, J.C. Martinou, Inhibition of Bax channel-forming activity by Bcl-2, Science 277 (1997) 370–372.
[18] P.H. Schlesinger, A. Gross, X.M. Yin, K. Yamamoto, M. Saito, G. Waksman, S.J. Korsmeyer, Comparison of the ion channel characteristics of proapoptotic BAX and antiapoptotic BCL-2, Proc. Natl. Acad. Sci. U. S. A. 94 (1997) 11357–11362.
[19] J.M. Jurgensmeier, Z. Xie, Q. Deveraux, L. Ellerby, D. Bredesen, J.C. Reed, Bax directly induces release of cytochrome c from isolated mitochondria, Proc. Natl. Acad. Sci. U. S. A. 95 (1998) 4997–5002.
[20] M. Saito, S.J. Korsmeyer, P.H. Schlesinger, BAX-dependent transport of cytochrome c reconstituted in pure liposomes, Nat. Cell Biol. 2 (2000) 553–555.
[21] X. Roucou, T. Rostovtseva, S. Montessuit, J.C. Martinou, B. Antonsson, Bid induces cytochrome c-impermeable Bax channels in liposomes, Biochem. J. 363 (2002) 547–552.
[22] K.G. Wolter, Y.T. Hsu, C.L. Smith, A. Nechushtan, X.G. Xi, R.J. Youle, Movement of Bax from the cytosol to mitochondria during apoptosis, J. Cell Biol. 139 (1997) 1281–1292.
[23] A. Nechushtan, C.L. Smith, Y.T. Hsu, R.J. Youle, Conformation of the Bax C-terminus regulates subcellular location and cell death, EMBO J. 18 (1999) 2330–2341.
[24] R.J. Boohaker, G. Zhang, A.L. Carlson, K.N. Nemec, A.R. Khaled, BAX supports the mitochondrial network, promoting bioenergetics in nonapoptotic cells, Am. J. Physiol. Cell Physiol. 300 (2011) C1466–C1478.
[25] O. Terrones, B. Antonsson, H. Yamaguchi, H.G. Wang, J. Liu, R.M. Lee, A. Herrmann, G. Basanez, Lipidic pore formation by the concerted action of proapoptotic BAX and tBID, J. Biol. Chem. 279 (2004) 30081–30091.
[26] T. Kuwana, M.R. Mackey, G. Perkins, M.H. Ellisman, M. Latterich, R. Schneiter, D.R. Green, D.D. Newmeyer, Bid, Bax, and lipids cooperate to form supramolecular openings in the outer mitochondrial membrane, Cell 111 (2002) 331–342.
[27] M. Suzuki, R.J. Youle, N. Tjandra, Structure of Bax: coregulation of dimer formation and intracellular localization, Cell 103 (2000) 645–654.
[28] M. del Mar Martinez-Senac, S. Corbalan-Garcia, J.C. Gomez-Fernandez, Conformation of the C-terminal domain of the pro-apoptotic protein Bax and mutants and its interaction with membranes, Biochemistry 40 (2001) 9983–9992.
[29] A. Torrecillas, M.M. Martinez-Senac, A. Ausili, S. Corbalan-Garcia, J.C. Gomez-Fernandez, Interaction of the C-terminal domain of Bcl-2 family proteins with model membranes, Biochim. Biophys. Acta 1768 (2007) 2931–2939.

[30] R.J. Boohaker, G. Zhang, M.W. Lee, K.N. Nemec, S. Santra, J.M. Perez, A.R. Khaled, Rational development of a cytotoxic peptide to trigger cell death, Mol. Pharm. 9 (2012) 2080–2093.
[31] S. Qin, A.H. Pande, K.N. Nemec, S.A. Tatulian, The N-terminal alpha-helix of pancreatic phospholipase A_2 determines productive-mode orientation of the enzyme at the membrane surface, J. Mol. Biol. 344 (2004) 71–89.
[32] F.N. Fu, B.R. Singh, Calcein permeability of liposomes mediated by type A botulinum neurotoxin and its light and heavy chains, J. Protein Chem. 18 (1999) 701–707.
[33] C. Snider, S. Jayasinghe, K. Hristova, S.H. White, MPEx: a tool for exploring membrane proteins, Protein Sci. 18 (2009) 2624–2628.
[34] D. Rapaport, R. Peled, S. Nir, Y. Shai, Reversible surface aggregation in pore formation by pardaxin, Biophys. J. 70 (1996) 2502–2512.
[35] S.C. Park, J.Y. Kim, S.O. Shin, C.Y. Jeong, M.H. Kim, S.Y. Shin, G.W. Cheong, Y. Park, K.S. Hahm, Investigation of toroidal pore and oligomerization by melittin using transmission electron microscopy, Biochem. Biophys. Res. Commun. 343 (2006) 222–228.
[36] G. Klocek, T. Schulthess, Y. Shai, J. Seelig, Thermodynamics of melittin binding to lipid bilayers. Aggregation and pore formation, Biochemistry 48 (2009) 2586–2596.
[37] M. Vogel, C. Munster, W. Fenzl, T. Salditt, Thermal unbinding of highly oriented phospholipid membranes, Phys. Rev. Lett. 84 (2000) 390–393.
[38] J. Seelig, S. Nebel, P. Ganz, C. Bruns, Electrostatic and nonpolar peptide–membrane interactions. Lipid binding and functional properties of somatostatin analogues of charge $z=+1$ to $z=+3$, Biochemistry 32 (1993) 9714–9721.
[39] A.J. García-Sáez, I. Mingarro, E. Pérez-Payá, J. Salgado, Membrane-insertion fragments of Bcl-x_L, Bax, and Bid, Biochemistry 43 (2004) 10930–10943.
[40] S. Nir, J.L. Nieva, Interactions of peptides with liposomes: pore formation and fusion, Prog. Lipid Res. 39 (2000) 181–206.
[41] J.L. Nieva, A. Agirre, S. Nir, L. Carrasco, Mechanisms of membrane permeabilization by picornavirus 2B viroporin, FEBS Lett. 552 (2003) 68–73.
[42] R.A. Parente, S. Nir, F.C. Szoka Jr., Mechanism of leakage of phospholipid vesicle contents induced by the peptide GALA, Biochemistry 29 (1990) 8720–8728.
[43] P.W. Atkins, Physical Chemistry, W.H. Freeman and Company, New York, 1999.
[44] P.F.F. Almeida, W.L.C. Vaz, Lateral diffusion in membranes, in: R. Lipowsky, E. Sackmann (Eds.), Structure and Dynamics of Membranes: From Cells to Vesicles, Elsevier, Amsterdam, 1995, pp. 305–357.
[45] S. Lee, G.S. Chirikjian, Interhelical angle and distance preferences in globular proteins, Biophys. J. 86 (2004) 1105–1117.
[46] S. Arnott, S.D. Dover, A. Elliott, Structure of beta-poly-L-alanine: refined atomic co-ordinates for an anti-parallel beta-pleated sheet, J. Mol. Biol. 30 (1967) 201–208.
[47] A.R. Fersht, J.P. Shi, J. Knill-Jones, D.M. Lowe, A.J. Wilkinson, D.M. Blow, P. Brick, P. Carter, M.M. Waye, G. Winter, Hydrogen bonding and biological specificity analysed by protein engineering, Nature 314 (1985) 235–238.
[48] D.H. Williams, M.S. Searle, J.P. Mackay, U. Gerhard, R.A. Maplestone, Toward an estimation of binding constants in aqueous solution: studies of associations of vancomycin group antibiotics, Proc. Natl. Acad. Sci. U. S. A. 90 (1993) 1172–1178.
[49] A.J. Garcia-Saez, M. Coraiola, M. Dalla Serra, I. Mingarro, G. Menestrina, J. Salgado, Peptides derived from apoptotic Bax and Bid reproduce the poration activity of the parent full-length proteins, Biophys. J. 88 (2005) 3976–3990.
[50] A.J. Garcia-Saez, M. Coraiola, M.D. Serra, I. Mingarro, P. Muller, J. Salgado, Peptides corresponding to helices 5 and 6 of Bax can independently form large lipid pores, FEBS J. 273 (2006) 971–981.
[51] J. Zimmerberg, R. Blumenthal, D.P. Sarkar, M. Curran, S.J. Morris, Restricted movement of lipid and aqueous dyes through pores formed by influenza hemagglutinin during cell fusion, J. Cell Biol. 127 (1994) 1885–1894.
[52] F. Nicol, S. Nir, F.C. Szoka Jr., Effect of cholesterol and charge on pore formation in bilayer vesicles by a pH-sensitive peptide, Biophys. J. 71 (1996) 3288–3301.
[53] Z. Chang, Y. Luo, Y. Zhang, G. Wei, Interactions of Aβ25-35 β-barrel-like oligomers with anionic lipid bilayer and resulting membrane leakage: an all-atom molecular dynamics study, J. Phys. Chem. B 115 (2011) 1165–1174.
[54] G. Agner, Y.A. Kaulin, P.A. Gurnev, Z. Szabo, L.V. Schagina, J.Y. Takemoto, K. Blasko, Membrane-permeabilizing activities of cyclic lipodepsipeptides, syringopeptin 22A and syringomycin E from *Pseudomonas syringae pv. syringae* in human red blood cells and in bilayer lipid membranes, Bioelectrochemistry 52 (2000) 161–167.
[55] N. Saint, L. Marri, D. Marchini, G. Molle, The antibacterial peptide ceratotoxin A displays alamethicin-like behavior in lipid bilayers, Peptides 24 (2003) 1779–1784.
[56] S. Wen, M. Majerowicz, A. Waring, F. Bringezu, Dicynthaurin (ala) monomer interaction with phospholipid bilayers studied by fluorescence leakage and isothermal titration calorimetry, J. Phys. Chem. B 111 (2007) 6280–6287.
[57] F. Nicol, S. Nir, F.C. Szoka Jr., Orientation of the pore-forming peptide GALA in POPC vesicles determined by a BODIPY-avidin/biotin binding assay, Biophys. J. 76 (1999) 2121–2141.
[58] M.L. Mangoni, Y. Shai, Short native antimicrobial peptides and engineered ultrashort lipopeptides: similarities and differences in cell specificities and modes of action, Cell. Mol. Life Sci. 68 (2011) 2267–2280.